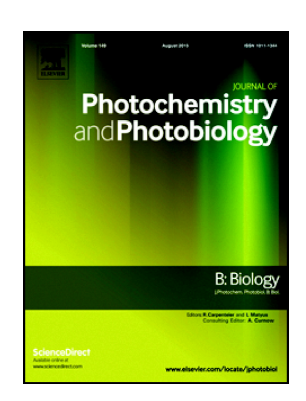
Transient absorption spectroscopy to explore cellular pathways to photobiomodulation

Sean P. O'Connor, Samantha M. Powell, John M. Rickman, Nathaniel J. Pope, Gary D. Noojin, Marlan O. Scully, Michael L. Denton, Vladislav V. Yakovlev



PII: S1011-1344(21)00150-0

DOI: https://doi.org/10.1016/j.jphotobiol.2021.112271

Reference: JPB 112271

To appear in: Journal of Photochemistry & Photobiology, B: Biology

Received date: 8 January 2021

Revised date: 15 July 2021

Accepted date: 20 July 2021

Please cite this article as: S.P. O'Connor, S.M. Powell, J.M. Rickman, et al., Transient absorption spectroscopy to explore cellular pathways to photobiomodulation, *Journal of Photochemistry & Photobiology*, *B: Biology* (2018), https://doi.org/10.1016/j.jphotobiol.2021.112271

This is a PDF file of an article that has undergone enhancements after acceptance, such as the addition of a cover page and metadata, and formatting for readability, but it is not yet the definitive version of record. This version will undergo additional copyediting, typesetting and review before it is published in its final form, but we are providing this version to give early visibility of the article. Please note that, during the production process, errors may be discovered which could affect the content, and all legal disclaimers that apply to the journal pertain.

© 2018 © 2021 Published by Elsevier B.V.

Transient absorption spectroscopy to explore cellular pathways to photobiomodulation

Sean P. O'Connor^{a,1}, Samantha M. Powell^{b,1,2}, John M. Rickman^c, Nathaniel J. Pope^{c,d}, Gary D. Noojin^c, Marlan O. Scully^{a,e}, Michael L. Denton^{f,*} michael.denton.10@us.af.mil, and Vladislav V. Yakovlev^{a,g,*} yakovlev@tamu.edu

Abstract

Photobiomodulation (PBM) describes the use of low irradiance light in the and to near-infrared wavelength range to stimulate biological effects in tissue, and many biological and spectro-copic techniques are used to study PBM. However, these techniques focus on the products or downstrean, effects rather than the electronic transitions that initiate the PBM processes. This study presents a novel approach a studying low irradiance light exposures on individual proteins and/or protein complexes by combining a continuous wave (CW) laser diode with femtosecond transient absorption spectroscopy (TAS), coined here as CV-T as, and tests the system on reduced cytochrome c (Cyt c) for proof of principle.

TAS was conducted using a 532-nm excitation put beam and a 350-600 nm supercontinuum probe. CW laser diodes with wavelengths of 450 nm, 635 nm, and 808 nm were interchangeably fiber coupled into the HELIOS Fire. Samples of Cyt c were tested by TAS using a pump power of 15 μW, both with and without CW exposure. CW exposures were carried out with irradiances of 1.00 and 3.20 mW/cm², except for 808 nm, which was only tested at 1.60 mW/cm². Both kinetic and global analyses were performed on the TAS data and the time constants for sets with and without CW exposures were compared.

The TAS data for Cyt c with the full decage of CW exposures did not alter the TAS data distinguishably from the control data. No new electronic transies signals were observed beyond the background when testing Cyt c with the CW exposures. Kinetic analysis, and that existing transients did not deviate beyond uncertainty. Global time constants for Cyt c were colounted to be 0.25 ± 0.03 ps and 5.1 ± 0.3 ps for the control study, and the time constants for the CW exposed Cyt c were not significantly different.

This study concludes that CW irradiation, at doses delivered, does not alter the transient absorption data of Cyt c. The CW-TAS method provides a new tool for studying PBM effects in other proteins and protein complexes that might respond to the CW wavelengths, such as Complex IV, in future studies.

Keywords

photobiomodulation, low-level light, low-level laser, transient absorption spectroscopy, cytochrome c

1. Introduction

^aDepartment of Physics and Astronomy, Texas A&M University, College Station, TX 77843

^bNational Research Council, AFRL, JBSA Fort Sam Houston, TX 78234

^cSAIC, 4141 Petroleum Road, JBSA Fort Sam Houston, TX 78238

^dOak Ridge Institute of Science and Education, AFRL, JBSA Fort Sam Houston, TX 78234

^eDepartment of Physics, Baylor University, Waco, TX 76798

^fAFRL, JBSA Fort Sam Houston, TX 78234

^gDepartment of Biomedical Engineering, Texas A&M University, College Staticr, TX 77843

^{*}Corresponding authors.

¹ These authors contributed equally to this work and should be considered as joint first authors.

² Present address: Biological Sciences Division, Pacific Northwest National Laboratory, Richland, WA 99352

Photobiomodulation (PBM) utilizes low irradiance light in the red to near-infrared (NIR) wavelength range (R-NIR) to generate beneficial biological effects in living cells and tissues. One early study of PBM showed that exposing cells to a low-power 632.8-nm HeNe laser stimulated ATP synthesis in mitochondria [1]. Since then, a wide range of methodologies have been used to study the effects of PBM, ranging from biological methods such as histology [2] and western blot analysis [3], to the techniques of spectrophotometry [4], Raman spectroscopy [5], and fluorescence [6]. Many of these studies focus on the products, or downstream effects of cellular processes, rather than the immediate photon absorption steps by proteins that initiate the PBM processes. Some beneficial physiological outcomes from PBM include enhanced wound healing [7–9], pain relief [10,11], cell proliferation [12], and reduction of both inflammation [13] and muscular soreness [14], as well as increased muscular performance, resistance to muscle fatigue [15], nerve regeneration [16–18], and mitigation of traumat. brain injury [19].

Mitochondria, the chief producers of ATP in eukaryotic cells, are generally accepted as critical targets of PBM therapy [20]. The leading hypothesis for the origin of the PBM effect points specifically towards an enzyme complex in the electron transport chain (ETC). The absorption profile of Complex IV (C-IV) has several similarities while the action spectrum for PBM and has been named the primary photoreceptor for PBM therapies [21–26]. However, other ETC proteins, namely Complex III (C-III) and cytochrome c (Cyto), share some of the absorption properties of C-IV, and are often found bound together in real imeric supercomplexes. Therefore, it is important to widen the focus of PBM research to include C-III and Cyt c as potential targets of PBM therapies.

The primary role of Cyt c in the ETC 1. to shuttle electrons between C-III and C-IV, and in the process, pump protons across the mitochondrial membrane to contribute to the electrochemical proton gradient that drives the synthesis of ATP [27,28]. C-III, C-IV, and Cyt c are heme-containing proteins. Heme group, are iron-containing porphyrins whose absorption spectra are characterized by a strong absorption peak in the Soret band (~380 - 500 nm), and weaker absorption peaks in the Q band (~500 - 700 nm) [29]. The ability of these proteins to shuttle electrons, in combination with the fact that heme proteins are easily characterized by spectroscopic techniques [29], also make C-III, C-IV, and Cyt c potential candidates for involvement in PBM. This, light-dependent perturbations in the electronic transitions of these three photoactive proteins would implicate them in the initiation of PBM pathways.

Light-induced electronic excitations in proteins can be on the order of femtoseconds (fs) to picoseconds [30,31], thus requiring the use of a femtosecond laser source to obtain the necessary temporal resolution for resolving these dynamics with spectroscopy. Ultrafast spectroscopic methods, such as fs transient absorption spectroscopy (TAS) are ideal for studying short-lived photoinduced energy and electron transfers, such as those expected at the beginning of the signaling pathways associated with PBM. Applying light exposures, consistent with those used in PBM studies to individual ETC proteins during TAS data collection, could eliminate or implicate these proteins for involvement in the PBM response.

TAS is a pump-probe spectroscopic technique that can characterize the photophysical dynamics of biological and chemical systems. In TAS, if the sample contains molecules that absorb

photons at the pump wavelength, a single ultrashort pulse from the pump promotes a fraction of the chromophore's electrons into a transient excited state. At various delay times relative to the pump pulse [32], a single probe pulse of supercontinuum light provides a broadband absorption measurement of the sample. Typically, both the pump and probe pulses have durations of about 100 fs. As the time delay is varied, and if the transient electronic states have a unique absorption wavelength relative to the ground state absorption profile, the method identifies absorption lifetime dynamics that are specific to the chromophore and type of photoproduct generated. This process is repeated multiple times, changing the time delay each time, until all transients have either transferred their energy or decayed back to the ground state.

To normalize the transient spectra, the pump probe is delivered at one-half the frequency of the probe pulses, and those absorption measurements without a preculing pump pulse make up the dynamic ground state absorption spectra. In real time with the probe pulses, the ground state absorption value (without pump) is subtracted from the excited state absorption (with pump pulse preceding) to obtain an absorbance difference (ΔA) at each delay time. Over the course of the measurement, a complete ΔA profile, as a function of the wavelength and time delay ($\Delta A(\lambda, t)$), is generated.

Even though there is a generally accepted hypothes's to, the PBM process that begins with electronic transitions in C-IV [21,23], others have reported the possibility of a photophysical mechanism whereby R-NIR light reduces in accoular water viscosity [33]. Addressing the question of an electronic excitation mechanism, we have modified the TAS method to include a third laser beam incident on the same sample volume interrogated by the pump and probe beams. Here, this third beam has wavelength and irradiance (W/cm²) dosimetry consistent with those giving rise to release of nitric oxid: NO) in retinal pigment epithelial cells in culture [6]. Whether this release of NO is an early to p in the path to PBM remains unknown, but neither NO release nor PBM effects occur namediately upon exposure to light. This implies a delayed metabolic response. Thus, when 'poking for immediate light-induced effects in purified proteins, or even isolated mitochondria, w. are cautious about calling the applied low-irradiance CW light a "PBM light" because u.'s would imply a known down-stream effect. Our new TAS configuration allowed is a rerform TAS in real time with low-irradiance exposures, during the accumulation of radiant exposure. Although TAS has been used to probe the excited state dynamics of C-III [34,35], Cyt c [36-38], and C-IV [39], none of these studies assessed the effects an additional beam of light in real time with TAS data collection, such as R-NIR lowirradiance light.

In this study, we describe a modified TAS method that combines a 532-nm pump beam, a 350-600 nm supercontinuum probe, and an experimental beam of varying continuous wave (CW) irradiances at either 450 nm, 635 nm, or 808 nm to interrogate Cyt c in its reduced form. The focus of this study will be on Cyt c because it is a much smaller and less challenging protein to work with than C-IV, thus allowing us to establish a proof of concept for future studies focusing on C-IV. Because PBM effects at the system level require a certain time of exposure, our hypothesis is that capturing successive TAS data in real time with the CW laser will capture a time-dependent "switch" in the electrodynamics of the purified photoactive proteins that are

suspected of being responsive to the CW wavelength. In this manner, we also demonstrate that this concomitant CW exposure does not degrade or interfere with the TAS signal. We believe the described method to be useful in characterizing photoresponsive proteins or enzyme complexes. The application of this technique, which we call CW-TAS, to the components of the ETC will allow us to identify whether R-NIR low-level light can induce electronic transitions in the enzyme complexes implicated in PBM.

2. Methods

2.1 Sample Preparation

Cytochrome c was purchased from Sigma-Aldrich and used without further purification. Samples (0.8 mM) of oxidized cytochrome c (Cyt c_{ox}) were prepared by n. xing solid Cyt c in a 25 mM NaPO₄, pH 6.3 buffer containing 0.14 M NaCl. To prepare same less of the reduced form (Cyt c_{red}), a small amount of solid dithionite was added to the solution of Cyt c_{ox}. The sample was centrifuged briefly to remove excess solid. The oxidation state of all samples was verified by UV-VIS spectroscopy using a Cary 6000i spectrophotometer prior to all TAS experiments. Samples were assayed in a quartz cuvette with a 2-mm path length.

2.2 Transient Absorption Spectrometer Setup

All TAS experiments were performed with a FLIOS Fire (Ultrafast Systems) transient absorption spectrometer, and Figure 1 disr a, s a schematic of the HELIOS system. The pump and probe sources were provided by a Ti:s, whire regenerative amplifier (SpitFire Ace, Spectra-Physics) with wavelength centered at 900 nm, pulse duration of 80 fs, and repetition rate of 1 kHz. The pump pulses were generated by politting part of the 800-nm source light to an optical parametric amplifier (OPA; TOPAS-Γ vi is, Light Conversion), where it was converted to 532nm light (FWHM ~10 nm) by the method discussed in previous studies [40,41]. The pump light traveled through a chopper wheel (CW, Fig. 1) that reduced the repetition rate to 500 Hz. The pump pulses were focused with a converging lens (L1, Fig. 1) and directed to be coincident with the probe pulses within the sample (S, Fig. 1). The probe pulse consisted of a supercontinuum (350-600 nm) generated from the fundamental 800-nm pulse incident upon a window of CaF₂ (W, Fig. 1), also having a repetition rate of 1 kHz. After the supercontinuum probe was generated, the center of the probe beam passed through a through-hole in the first parabolic mirror (PM1, Fig. 1) to eliminate the majority of the remaining 800 nm. The remaining annular shaped probe continued to the next parabolic mirror (PM2, Fig. 1). This light passed through an 800-nm notch filter (F, Fig. 1) to remove the residual 800 nm. The second parabolic mirror redirected and focused the probe pulse into the beam path of the pump pulse. The foci of the pump and probe pulses converged at the same volume within the sample (S, Fig. 1), and the annular shape of the probe beam kept it from overlapping with the pump until it reached the sample. After passing through the sample, the pump and probe pulses approached the third parabolic mirror (PM3, Fig. 1) with a through-hole which allowed the pump pulse to pass through and collimated the annular-shaped probe pulse. The final parabolic mirror (PM4, Fig. 1) focused the probe pulse into the collection fiber (CF, Fig. 1). The beam radius of the pump pulse

was about 100 μ m at its focal point, as determined by the knife-edge technique [42] assuming a $1/e^2$ beam waist.

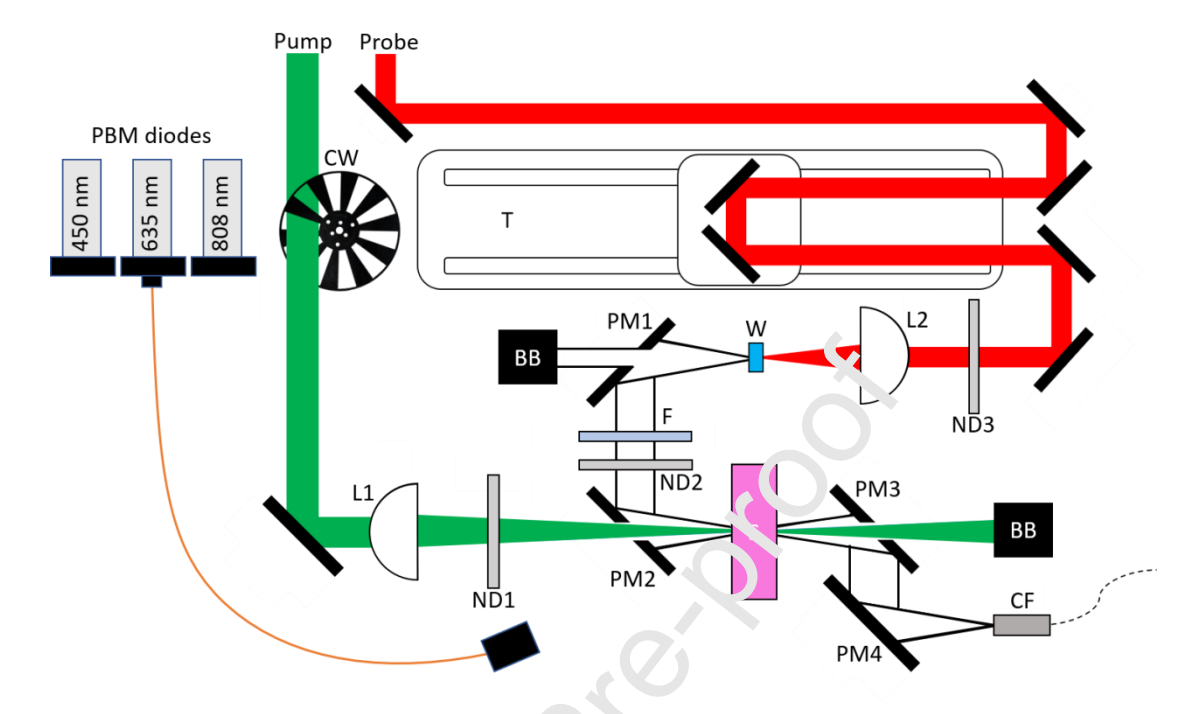


Fig. 1. Schematic for the HELIOS Fire fs tra sien absorption spectrometer. BB denotes the beam blocks. CF is the collection fiber connecting to the spect ometer. CW is the chopper wheel. F is the 800-nm filter. PM1, PM2, PM3, and PM4 are off-axis p. abolic mirrors. L1 and L2 are converging lenses. ND1, ND2, and ND3 are neutral density filters. S is the sample. T is the translation stage. W is the window of CaF₂.

As shown in Figure 2, the CaF₂ window generated a supercontinuum in the ultraviolet to visible (UV-VIS) region. The CaF₂ crystal was kept in motion through translation to maintain the stability of the supercontinuum output and to prevent damage from the incident 800-nm pulses [43].

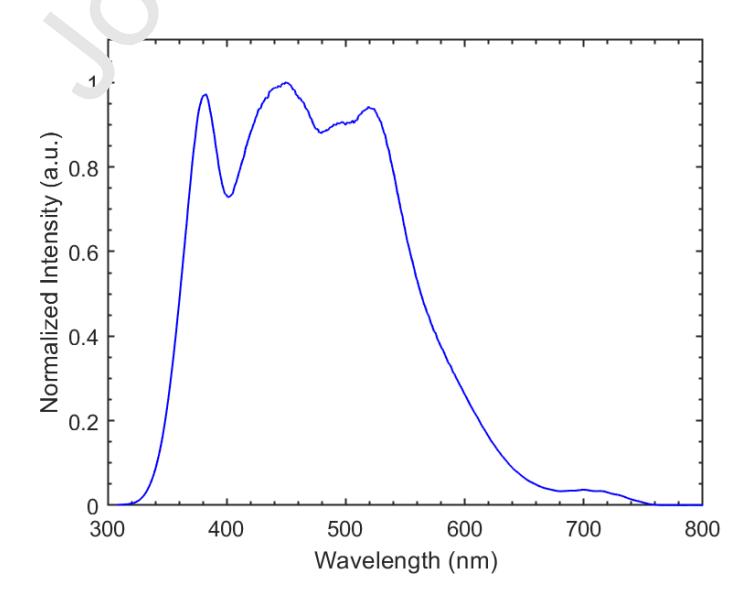


Fig. 2. Supercontinuum spectra generated from the CaF₂ window.

2.3 Low-Irradiance CW Laser Diode Setup

For sample irradiation with low-irradiance CW lasers during TAS scanning, the output from one of three laser diodes was coupled into a fiber imaging system (Fig. 1) that was mounted in the transient absorption spectrometer. We used CW laser diodes (Thorlabs) with wavelengths of 450 nm (blue; CPS450), 635 nm (red; CPS635), or 808 nm (NIR; CPS808A) that were all interchangeably coupled into a 550- μ m diameter fiber (M37L02, Thorlabs). The output power of the diodes was controlled with a continuously variable neutral density filter (NDL-25C-2, Thorlabs) prior to the coupling of the light into the fiber. The fiber output was imaged to the sample with a flat top beam profile having a diameter of 0.95 cm, resulting in an area of 0.71 cm² at the cuvette. The fiber output was placed above the pump, probe beam plane, and directed to the cuvette at a shallow angle so that the diode light was not collected by the parabolic mirror (PM3, Fig. 1) beyond the sample. The light from the laser divided illuminations did not affect the $\Delta A(\lambda, t)$ spectrum, as verified through observation of the real time $\Delta A(\lambda)$ spectrum in the HELIOS software.

2.4 Testing Parameters

For the TAS procedure, the 532-nm pump wavelength was used with a power of 15 µW, and the UV-VIS supercontinuum was used for the pulse. The pump and probe pulse overlap was optimized before the start of each TAS measurement by testing with a 0.36 mM Rhodamine 6G in methanol solution and maximizing the signal response using the Helios spectrometer. The time delay setup for each scan was rogrammed to take 0.2-ps steps from -2 to 0 ps, 0.05-ps steps from 0 to 3 ps, 0.1-ps steps from 10 to 50 ps, for a total of 221 time steps. At each time delay tep, 0.5 s of measurement were taken, which resulted in 250 $\Delta A(\lambda, t)$ measurements averaged eigether at that time delay. The TAS program was set to take a total of 14 contiguous time same for each replicate of Cyt c tested. The first scan was taken as a baseline and did not have an 'CW laser diode light incident upon the sample. Scans 2-11 were taken with a CW diode muting light onto the Cyt c sample. Scans 12-14 were taken with the CW diode turned off to deserve changes after the full dosage of irradiation [6]. The total time to record 14 scans was 46 min and 36 ± 11 s. The duration of the CW diode exposure during scans 2-11 was computed to be 33 min and 17 ± 8 s. A detailed analysis was done to determine the number of necessary data sets to be collected in order to have a sufficient signal to noise ratio (See supplemental section S1.) and it was determined that five sets was sufficient. Five CW-TAS data sets were collected with each laser diode at each irradiance specified in Table 1, with the exception of the red laser diode at 3.20 mW/cm² where six sets were collected. The visible CW laser studies were conducted individually with an irradiance of either 1.60 or 3.20 mW/cm². Exposures at 808-nm were at 1.60 mW/cm² due to its maximum power constraint of 2.78 mW/cm^2 .

Laser Diode	CPS450		CPS635		CPS808A
Irradiance (mW/cm ²)	1.60	3.20	1.60	3.20	1.60
Total Power (mW)	1.13	2.27	1.13	2.27	1.13
Radiant Exposure (J/cm ²)	$3.20 \pm .01$	$6.39 \pm .03$	$3.20 \pm .01$	$6.39 \pm .03$	$3.20 \pm .01$
Total Energy (J)	$2.26 \pm .01$	$4.53 \pm .02$	$2.26 \pm .01$	$4.53 \pm .02$	$2.26 \pm .01$

Table 1. Laser diode parameters used for CW-TAS of Cyt c samples.

2.5 Data Processing and Analysis

Data was collected and exported from the Helios FIRE soft vare and processed in Surface Xplorer (version 4.3.0, Ultrafast Systems). Background subtractions were performed using the spectra taken at the time delays prior to time-zero. Chirp correction was performed for each data set, and the time-zero correction was acquired by fitting the coherence spiking near the zero delay time in the surface data. CW data sets were processed by averaging together each scan from a replicate sample to the same scan number from other replicate data collections. Then, the averaged baseline data were taken and compared to the averaged scan number 11, when the maximum amount of CW radiant exposure was delivered. Kinetic cross sections were taken at wavelength 374, 415, 430, and 570 nm, and the absorption difference kinetics of the full dosage scan was compared to the baseline kinetics.

Kinetic and global analyses were cordinated in Surface Xplorer. Kinetic fits were computed by the software using a sum of expensival decays convolved with a Gaussian instrumentation response function (IRF), as detailed in previous studies [44].

$$C(t) = e^{-\left(\frac{-t_0}{t_i}\right)^2} * \sum_i A_i e^{-\frac{t-t_0}{\tau_i}}, \qquad t_p = \frac{w_{FWHM}}{2 \ln 2} \#(1)$$

Equation 1 displays the k, retic model, C(t), as a function of time (t) between the pump and probe pulses, where \ast indicates convolution. In the equation, A_i is the magnitude contribution of each exponential decay of time constant (τ_i) , t_0 is time-zero, and t_p is a fit parameter relating to the Gaussian IRF's full width at half maximum (FWHM) shown as w_{FWHM} . Global analysis was performed by first performing principle component analysis on surface data through singular value decomposition (SVD) as detailed in previous studies [45]. Equation 1 was then used on the selected principal components to acquire the time constants.

3. Results

3.1 TAS of Reduced Cytochrome c

TAS measures the absorbance of excited state transitions of electrons, so it is important to first establish the ground state absorbance of the sample. Figure 3 presents the ground state absorbance spectra of both reduced and oxidized Cyt c using the Cary spectrophotometer. Cyt c_{ox} had a strong absorption peak in the Soret band at 409 nm, and a single, broad absorption peak in the Q band at 530 nm. The Soret peak for Cyt c_{red} was red-shifted with a λ_{max} at 415 nm, and in the Q band region, there were two peaks at 520 nm and 550 nm. The 532-nm pump's bandwidth (FWHM ~10 nm) overlapped with the absorption peaks of both reduced and oxidized Cyt c and allowed for the excitation of both species. The reduced form of Cyt c was used for all TAS experiments in this study.

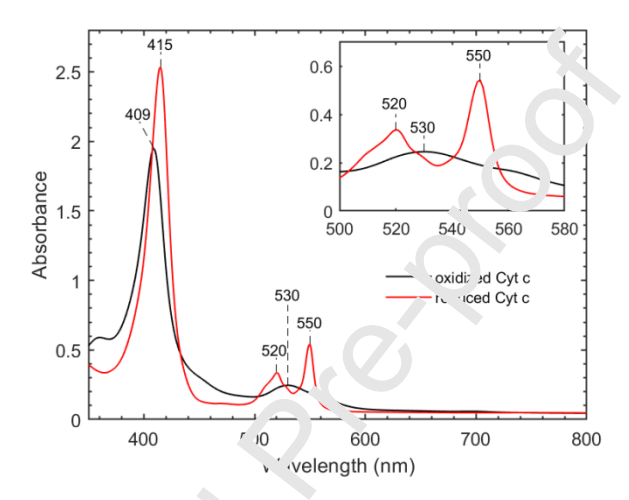


Fig. 3. Ground state absorbance spectra for Cvt c in its reduced (red) and oxidized (black) states. Inset plot displays a magnified view of the Q band

There are two possible changes in TAS data that would indicate light-induced electronic transitions had occurred. First subspecific absorption of one or a subspecific absorption of the low-level light. Second is a modification in a subspecific absorption of the low-level light. Once a subspecific absorption of the low-level light. Once a subspecific absorption of the low-level light, our analysis will provide valuable feedback for optimizing the dosimetry of the low-level light, and perhaps for the PBM response in general. From this information, we can further elucidate what underlying molecular processes are stimulated through PBM therapies.

TAS data collected for Cyt c in the Soret region using the 532-nm pump is shown in Figure 4a. The surface plot displayed positive transients (orange and red colors) at 374 nm and 429 nm, corresponding to excited state absorptions. More specifically, the 374-nm signal corresponded to changes in the heme δ band and the 429-nm signal corresponded to a ferrous five-coordinated heme [46]. The negative transient signal (blue color) at 415 nm corresponded to ground-state bleaching due to greater Soret band absorbance by Cyt c (Fig. 3). TAS data were also collected for the Q band using the 418-nm pump (Fig. S3), which displayed ground-state bleaching at around 520 nm and 550 nm. Figure 4b displays spectral cross sections over the Soret and Q bands taken at different time delays with the 532-nm pump scattering region not displayed. The ground-state bleaching at 550 nm was partially resolvable with the 532-nm excitation, but not

addressed further in kinetic analysis due to overlap with the 532-nm scattering region. Our TAS spectra agree with previous studies reported for reduced Cyt c [36–38].

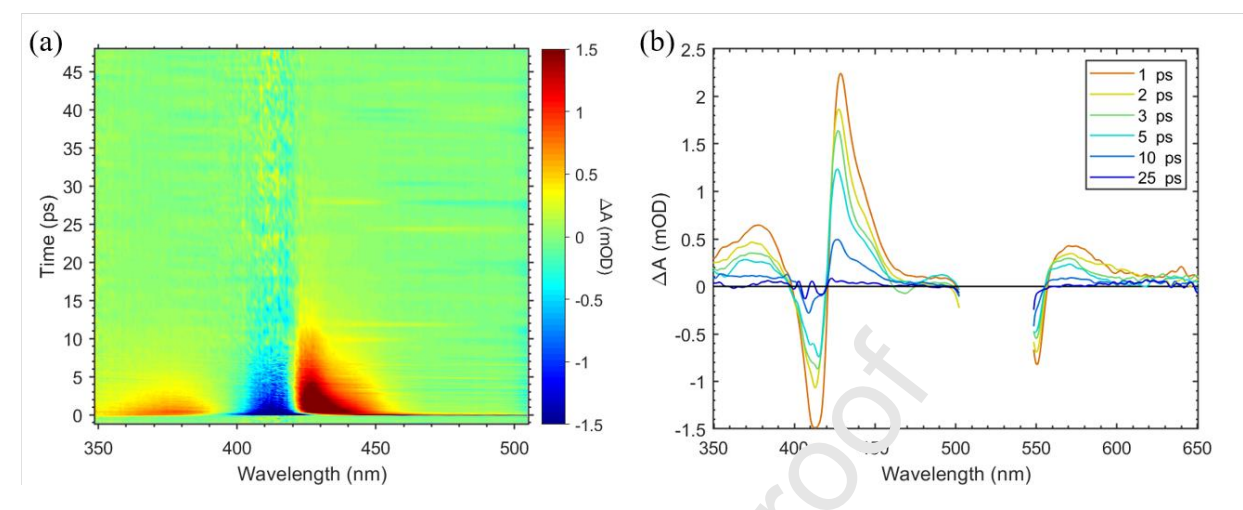


Fig. 4. Transient absorption spectra of Cyt c with 532-nm excitation at 30 nJ/pulse displayed as (a) a surface and (b) spectral cross sections at different time delays

3.2 CW-TAS comparison results – Kinetic Analy is

Comparisons between TAS data with and without CW light, made by examining kinetic cross sections of the surface data at wavelengths around local extrema of peaks (transients) and troughs (bleaching) appearing after the coherence spiking narraime-zero defined the data for comparison. Averaged kinetic data from the 11th scan with CW light was best for the comparison because this represented the time of delivery for maximum CW radiant exposure. Averaged kinetic data from the samples without CW light exposure provided the baseline for comparison with CW exposure. Figure 5 displays the comparisons of kinetic cross sections without and with 635-nm CW exposure at 3.20 mW/cm, asken at 373.6, 415.1, 429.5, and 569.6 nm. The normalized kinetic cross sections between the control data and CW data showed no significant deviation. Similar results (data not shown) were observed for the other CW wavelengths and irradiance settings listed in Table 1.

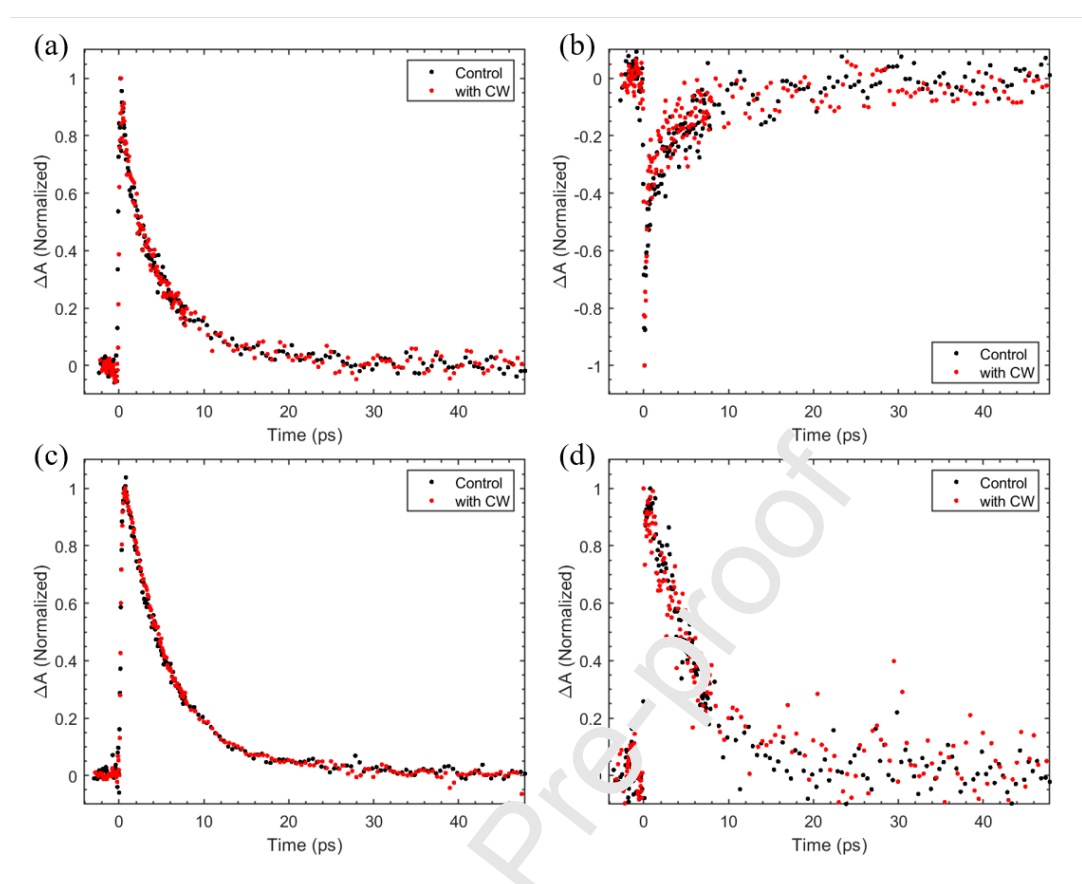


Fig. 5. Kinetic cross sections of Cyt c TA? data at (a) 373.6 nm, (b) 415.1 nm, (c) 429.5 nm, and (d) 569.6 nm, displaying the normalized transient respo. se both with (red) and without CW (black). Pump power was 30 nJ/pulse, and the CW light was from ne o.`5-nm diode at 3.20 mW/cm².

Surface Xplorer provided kinetic (it to the time constants in each cross section shown in Figure 5. Table 2 provides the compiled time constants, along with their uncertainties as computed at the 90% confidence interval. The time constants extracted from the data with full dosage CW light did not vary in a statistically significant way from the time constants of the data without CW light. This supports he dea that the relaxation and transition processes in Cyt c were not changed by the CW dosages used in this study, and this is further explored with more robustness with global analysis techniques (see section 3.3).

Table 2. Kinetic fit results for Cyt c. Control sets were calculated with n = 14, whereas CW data sets were calculated with n = 5, except in the case of 635-nm CW at 3.2 mW/cm² where n = 6.

Cross-Section Wavelength (nm)	CW Wavelength (nm)	CW Irradiance (mW/cm²)	τ ₁ (ps)	τ ₂ (ps)
	Control #1	-	4.4 ± 0.3	-
373.6 nm	Control #2	=	4.7 ± 0.5	-
	450	1.60	4.8 ± 0.5	-
	450	3.20	4.3 ± 0.4	-
	635	1.60	3.9 ± 0.6	-
	635	3.20	4.5 ± 0.3	-
	808	1.60	4.1 ± 0.4	-
415.1 nm	Control #1	-	0.22 ± 0.11	5.6 ± 1.2

	Control #2	-	0.19 ± 0.17	5.4 ± 1.4
	450	1.60	0.19 ± 0.42	4.8 ± 3.0
	450	3.20	0.20 ± 0.15	5.6 ± 2.9
	635	1.60	0.20 ± 0.19	4.8 ± 2.4
	635	3.20	0.23 ± 0.08	5.2 ± 1.8
	808	1.60	0.47 ± 0.38	5.4 ± 2.7
429.5 nm	Control #1	-	0.19 ± 0.09	4.9 ± 0.2
	Control #2	-	0.19 ± 0.08	4.9 ± 0.2
	450	1.60	0.19 ± 0.33	5.0 ± 0.2
	450	3.20	0.20 ± 0.07	4.8 ± 0.2
	635	1.60	0.21 ± 0.07	5.1 ± 0.2
	635	3.20	0.20 ± 0.05	5.2 ± 0.1
	808	1.60	0.20 ± 0.04	5.0 ± 0.2
	Control #1	-	$0.21 \pm \sqrt{23}$	5.9 ± 1.9
579.6 nm	Control #2	-	0.19 ± 0.2	6.5 ± 2.6
	450	1.60	0.19 = 0.17	5.0 ± 1.5
	450	3.20	0.20 ± 0.10	6.3 ± 1.5
	635	1.60	(20 ± 0.31)	5.5 ± 3.0
	635	3.20	$0.2 \text{u} \pm 0.22$	5.6 ± 2.0
	808	1.60	0.20 ± 0.16	5.4 ± 1.4

3.3 CW-TAS comparison results – Global Analysis

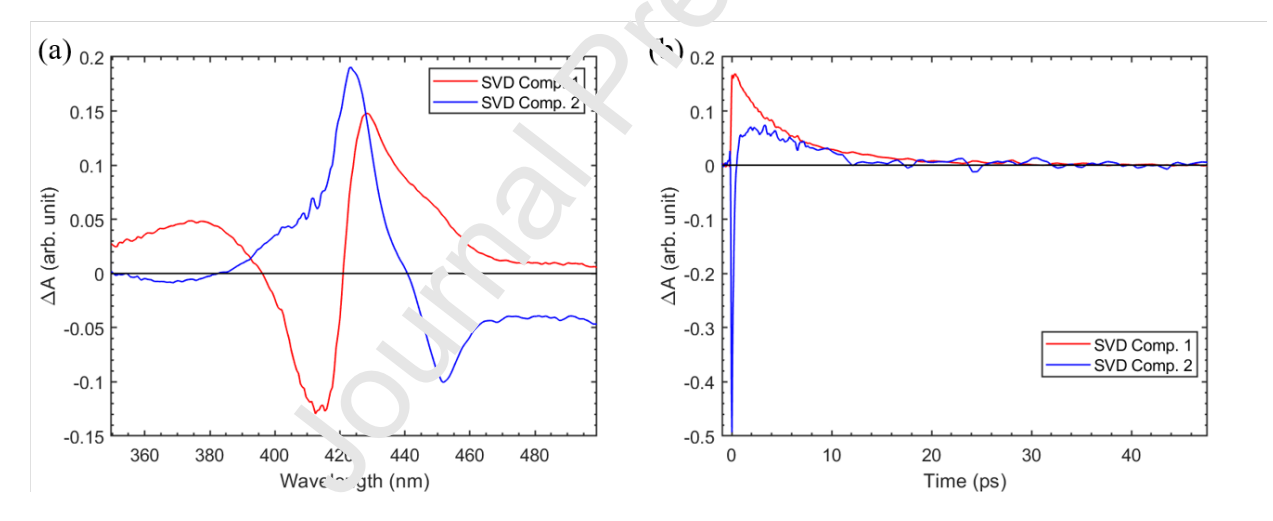


Fig. 6. The two significant (a) spectral components and (b) kinetic components from SVD analysis on the control data of Cyt c_{red} with the wavelength range of 350-500 nm.

We used global analysis to fit the time constants of the data sets of Cyt c, both with and without CW light exposure. The wavelength range chosen for the analysis was 350-500 nm. At shorter wavelengths, there was low signal to noise ratio (S/N) due to weak probe strength. At longer wavelengths, low S/N was due to pump pulse leakage into the detector. After performing SVD analysis on each TAS data set, two principle components were determined as significant for obtaining global time constants. For the control data, SVD analysis yielded singular values of $S_1 = 0.9$, $S_2 = 0.4$, and $S_k \le 0.1$ for $k \ge 3$. Figure 6 displays the first two principle spectra and kinetics. The principle kinetics were fit using Equation 1 and this resulted in the determination of two decaying exponential terms, along with a constant contribution. The time constants acquired

from global analysis on the control data were 0.25 ± 0.03 ps and 5.1 ± 0.3 ps. The global time constants for control and CW data collections are displayed in Table 3, along with their uncertainties computed at the 90% confidence interval. The time constants extracted using the global fitting procedure on the data with full dosage CW light did not vary in a statistically significant way from the data without CW light. Hence, the relaxation and transition processes associated with these time constants (detailed in the discussion) were unaffected by full dosage CW light.

Table 3. Global analysis fitting results for reduced Cyt c. Control sets were calculated with n = 14, whereas CW data sets were calculated with n = 5, except in the case of 635-nm CW at 3.20 mW/cm² where n = 6.

CW Wavelength (nm)	CW Irradiance (mW/cm²)	τ ₁ (ps)	τ ₂ (ps)
Control #1	-	0.25 ± 0.03	5.1 ± 0.3
Control #2	-	0.26 ± 0.03	5.1 ± 0.4
450	1.60	0.20 ± 0 11	5.3 ± 0.6
450	3.20	$0.20 \pm (05)$	5.0 ± 0.5
635	1.60	0.25 0.00	5.1 ± 0.5
635	3.20	0.20 0.33	5.0 ± 0.3
808	1.60	6.76 ± 0.05	4.9 ± 0.4

4. Discussion

4.1. Kinetic and Global Analyses

In our study, kinetic and global analyses of Cyt c yielded similar results, producing two time constants. We took both a kinetic and global analysis approach to analyzing TAS data of Cyt c, both without and with concurrent low-'evel CW light. Although more commonly used in pump-probe spectroscopies with a sing! wa relength probe pulse, kinetic analysis techniques can also be used to provide a first glimpte at the kinetic processes prior to global analysis. For broadband probe pulses, global analysis techniques are widely considered the standard approach for data analysis [44,45]. The longer that constant $(5.1 \pm 0.3 \text{ ps})$ is consistent with previous TAS studies on Cyt c using 532 nm e. citation [37]. The authors concluded this time constant corresponds to recombination of the distal methionine (Met-80) to the porphyrin Fe in the Cyt c active site. The shorter time constant $(0.25 \pm 0.03 \text{ ps})$ is consistent with the shorter relaxation values attributed to vibrational relaxation of the heme [36,37].

A time constant in the range of 2.5-2.8 ps was reported in previous studies [36,37], however, when the number of time constants used in our global analysis was increased, our SVD analysis did not resolve an approximately 2.5-ps time constant. In Wang *et al.*, the relative contribution of the 2.8-ps time constant is consistently weaker than the contributions from other time constants [36]. Additionally, in Negrerie *et al.*, the first SVD component is predominantly composed of the 4.8-ps time constant, and dwarfs the contribution from the 2.5-ps time constant [37]. Given that the noise level in our data at certain wavelengths is not optimal, as shown in Figure 5, it is likely that the 2.5-ps time constant could not be resolved due to the noise in the data. Therefore, to determine if the 2.5-ps time constant is resolvable in our samples, more replicates are needed to increase the signal-to-noise ratio (S/N). A longer (16 ps) time constant was also resolved by

Negrerie *et al.* [37]. Their study notes that the 16-ps time constant had a minor contribution compared to the 4.8-ps time constant, and their extended time window (out to 100 ps of time delay) helped them to further resolve the 16-ps time constant. Our analysis likely did not resolve the 16-ps time constant because the 16 ps time constant is a weaker contribution which requires higher S/N to resolve.

4.2. Effect of CW exposures on Cyt c TAS

In this study, both TAS and CW-TAS studies were performed on the reduced form of Cyt c. The choice of CW wavelength and dosimetry were meant to approximate exposures expected to generate PBM-like effects, based on results from previous studies [6,47]. In this way, we expected to identify whether Cyt c alone could account for the initial photon absorption and electronic state dynamics of PBM. We found that for low-level C V exposures at 450 nm, 635 nm, and 808 nm we could not distinguish any new transients (2A) reyond the noise floor in the TAS data. Additionally, we found no significant difference in the time constants for any transient signals due to CW illumination (Table 3). It is likely hat the reason that there are no measurable changes with the CW exposures is that the ground state absorption for Cyt c is weak at the wavelengths selected for the CW exposures. This leads us to eliminate Cyt c as a primary target of PBM with a mechanism of electronic transition. Alternatively, our results are consistent with a mechanism for PBM that does not require electronic excited states.

One limitation to our study was that we only proved the Soret region by using the 532-nm pump. Although we only did one control experiment to look at the Q band of Cyt c (Fig. S2), it is highly unlikely that probing within the Q band would have changed the outcome because any electronic change should affect *both* the Q and Scret regions [29].

Although we did not see an effect of CW light on the excited state dynamics of Cyt c, we did show that it is possible to successfully incorporate low-irradiance CW light into the Helios system without altering the TAS data. As presented in Tables 2 and 3, there were no statistically significant differences in electrodic state dynamics between our data sets with and without CW exposures as determined by both kinetic and global analyses. Finally, we have established the combined CW-TAS method as a viable method for screening proteins, or enzyme complexes, for potential involvement in the electronic initiation of PBM by careful choice of CW wavelength and dosimetry.

5. Conclusion

We have presented a modified method of TAS to include the introduction of steady-state CW laser exposure in real time with repeated TAS measurements. The CW irradiation did not alter the results of the TAS measurements using the reduced form of Cyt c. When using CW wavelengths and dosimetry reasonably expected to induce NO in cells, and potentially lead to PBM in animal systems, we were unable to identify electronic transients above background levels for Cyt c protein, likely due to the weak absorbance at the CW wavelengths utilized in our study. We hypothesize that electronic transitions will be induced for protein targets which do

have strong absorbance at the selected CW wavelength and these targets will be candidates for involvement in the initial step in the PBM process. To underpin our results with CW exposure, our kinetic and global analyses produced data consistent with that previously published. The CW-TAS method will provide a means for assessing other mitochondrial proteins and enzyme complexes for a role in PBM initiation via electronic transition.

Declaration of Competing Interest

The authors declare that they have no known competing financial interests of personal relationships that could have appeared to influence the work reported in this paper.

Acknowledgements

The authors would like to thank SAIC (Airman Systems Directorate, Contracts No. FA8650-14-D-6519 and FA8650-19-C-6024), and the US Air Force Pes arch Laboratory (AFRL). SPO was supported, in part, by the Herman F. Heep and Min ie Belle Heep Texas A&M University Endowed Fund held/administered by the Texas A M. Foundation, the Robert A. Welch Foundation (Grant No. A-1261), and by an approprient to the Student Research Participation Program (Repperger) at AFRL, administered by the Oak Ridge Institute for Science and Education (ORISE) through an interagency aga searent between the U.S. DoE and USAFRL. This research was performed while SMP held in NRC Research Associateship award and NJP was supported by the ORISE Postgraduate Research Participation Program. MOS acknowledges support from the Air Force Office of Scientific Research (AFOSR; FA9550-20-1-0366 DEF), the Office of Naval Research (ONR; N 0 0 14-20-1-2184), and the Robert A. Welch Foundation (Grant No. A-1261), and the National Science Foundation (NSF; PHY-2013771). MLD acknowledges support from AFOS? (19RHCOR067). VVY acknowledges partial funding from NSF (DBI-1455671, ECCS-150>?68, CMMI-1826078), AFOSR (FA9550-15-1-0517, FA9550-18-1-0141, FA9550-20-1-0266), Army Research Laboratory (W911NF-17-2-0144), DOD Army Medical Research (W81Y w 142010777), ONR (N00014-16-1-2578), NIH (1R01GM127696-01), and the Cancer Prevention and Research Institute of Texas (RP180588).

The opinions expressed in this document, electronic or otherwise, are solely those of the author(s). They do not represent an endorsement by or the views of the United States Air Force, the Department of Defense, or the United States Government. Approved for public release; distribution unlimited. PA Case No. TSRL-PA-2020-0192.

Distribution Statement A

Approved for public release; distribution is unlimited. TSRL-PA-2020-0192. The opinions expressed on this document, electronic or otherwise, are solely those of the author(s). They do not represent an endorsement by or the views of the United States Air Force, the Department of Defense, or the United States Government.

References

- [1] S. Passarella, E. Casamassima, S. Molinari, D. Pastore, E. Quagliariello, I.M. Catalano, A. Cingolani, Increase of proton electrochemical potential and ATP synthesis in rat liver mitochondria irradiated in vitro by helium-neon laser, FEBS Lett. 175 (1984) 95–99. https://doi.org/10.1016/0014-5793(84)80577-3.
- [2] N.M. Khalil, M.G. Noureldin, Comparison of Single Versus Multiple Low-Level Laser Applications on Bone Formation in Extraction Socket Healing in Rabbits (Histologic and Histomorphometric Study), J. Oral Maxillofac. Surg. 77 (2019) 1760–1768. https://doi.org/10.1016/j.joms.2019.03.037.
- [3] C.F. Rizzi, J.L. Mauriz, D.S. Freitas Corrêa, A.J. Moreira, C.G. Zettler, L.I. Filippin, N.P. Marroni, J. González-Gallego, Effects of low-level laser therapy (LLLT) on the nuclear factor (NF)-κB signaling pathway in traumatized muscle, Lasers Surg. Med. 38 (2006) 704–713. https://doi.org/10.1002/lsm.20371.
- [4] T. De Marchi, E.C.P. Leal Junior, C. Bortoli, S.S. Tomazoni, R.A. B. Lopes-Martins, M. Salvador, Low-level laser therapy (LLLT) in human progressive intensity running: effects on exercise performance, skeletal muscle status, and oxidative stress, Lasers Med. Sci. 27 (2012) 231–236. https://doi.org/10.1007/s10103-011-0955-5.
- [5] C.B. Lopes, A.L.B. Pinheiro, S. Sathaiah, N.S. Da Silva, M.A.C. Salgado, Infrared Laser Photobiomodulation (λ 830 nm) on Bone Tissue Aroung Dental Implants: A Raman Spectroscopy and Scanning Electronic Microscopy Study in Rabbits, Photomed. Laser Surg. 25 (2007) 96–101. https://doi.org/10.1089/pho.2006.2029.
- [6] N.J. Pope, S.M. Powell, J.C. Wigle, M.L. Dental, Wavelength- and irradiance-dependent changes in intracellular nitric oxide level, J. Pioned. Opt. 25 (2020) 1. https://doi.org/10.1117/1.JBO.25.8.085001
- [7] P. V Peplow, T. Chung, G.D. Baxter, Lasc Photobiomodulation of Wound Healing: A Review of Experimental Studies in Mouse and Rat Animal Models, Photomed. Laser Surg. 28 (2010) 291–325. https://doi.org/10.10/39 pho.2008.2446.
- [8] A.V. Corazza, J. Jorge, C. Kurachi, V.S. Bagnato, Photobiomodulation on the Angiogenesis of Skin Wounds in Rats Using Different Light Sources, Photomed. Laser Surg. 25 (2007) 102–106. https://doi.org/10.1089/phc.2006.2011.
- [9] J.M. Cordeiro, M.G. Sahad, M.F.X.B. Cavalcanti, R.L. Marcos, F. Diomede, O. Trubiani, D.A. Maria, E.C.P. Leal-Junio, L. Frigo, Laser Photobiomodulation Over Teeth Subjected to Orthodontic Movement, Photomed. Laser Surg. 36 (2018) 647–652. https://doi.org/10.1089/pi.o.2018.4532.
- [10] R.T. Chow, P.J. Ar. ati, Photobiomodulation: Implications for Anesthesia and Pain Relief, Photomed. Laser Surg. 34 (2016) 599–609. https://doi.org/10.1089/pho.2015.4048.
- [11] M.F.X.B. Cavalcanti, U.H. Silva, E.C.P. Leal-Junior, R.A.B. Lopes-Martins, R.L. Marcos, R.C. Pallotta, F. Diomede, O. Trubiani, N. De Isla, L. Frigo, Comparative Study of the Physiotherapeutic and Drug Protocol and Low-Level Laser Irradiation in the Treatment of Pain Associated with Temporomandibular Dysfunction, Photomed. Laser Surg. 34 (2016) 652–656. https://doi.org/10.1089/pho.2016.4195.
- [12] M.F.X.B. Cavalcanti, D.A. Maria, N. de Isla, E.C.P. Leal-Junior, J. Joensen, J.M. Bjordal, R.A.M.B. Lopes-Martins, F. Diomede, O. Trubiani, L. Frigo, Evaluation of the Proliferative Effects Induced by Low-Level Laser Therapy in Bone Marrow Stem Cell Culture, Photomed. Laser Surg. 33 (2015) 610–616. https://doi.org/10.1089/pho.2014.3864.
- [13] F.M. de Lima, A.B. Villaverde, R. Albertini, J.C. Corrêa, R.L.P. Carvalho, E. Munin, T. Araújo, J.A. Silva, F. Aimbire, Dual Effect of low-level laser therapy (LLLT) on the acute lung

- inflammation induced by intestinal ischemia and reperfusion: Action on anti- and proinflammatory cytokines, Lasers Surg. Med. 43 (2011) 410–420. https://doi.org/10.1002/lsm.21053.
- [14] P. Douris, V. Southard, R. Ferrigi, J. Grauer, D. Katz, C. Nascimento, P. Podbielski, Effect of Phototherapy on Delayed Onset Muscle Soreness, Photomed. Laser Surg. 24 (2006) 377–382. https://doi.org/10.1089/pho.2006.24.377.
- [15] C. Ferraresi, M.V.P. de Sousa, Y.-Y. Huang, V.S. Bagnato, N.A. Parizotto, M.R. Hamblin, Time response of increases in ATP and muscle resistance to fatigue after low-level laser (light) therapy (LLLT) in mice, Lasers Med. Sci. 30 (2015) 1259–1267. https://doi.org/10.1007/s10103-015-1723-8.
- [16] J.J. Anders, S. Geuna, S. Rochkind, Phototherapy promotes regeneration and functional recovery of injured peripheral nerve, Neurol. Res. 26 (2004) 233–739. https://doi.org/10.1179/016164104225013914.
- [17] J.J. Anders, H. Moges, X. Wu, I.D. Erbele, S.L. Alberico, F.K. Saidu, J.T. Smith, B.A. Pryor, In vitro and in vivo optimization of infrared laser treatment for injured peripheral nerves, Lasers Surg. Med. 46 (2014) 34–45. https://doi.org/10.1002/1/m.22212.
- [18] K.R. Byrnes, R.W. Waynant, I.K. Ilev, X. Wu, L. Barn, K. Smith, R. Heckert, H. Gerst, J.J. Anders, Light promotes regeneration and functional recovery and alters the immune response after spinal cord injury, Lasers Surg. Med. 36 (2005) 171-185. https://doi.org/10.1002/lsm.20143.
- [19] M.R. Hamblin, Photobiomodulation for trawn. ic brain injury and stroke, J. Neurosci. Res. 96 (2018) 731–743. https://doi.org/10.1002/j... 21190.
- [20] S. Passarella, T. Karu, Absorption of nor schromatic and narrow band radiation in the visible and near IR by both mitochondrial and non-mitochondrial photoacceptors results in photobiomodulation, J. Photochem. Phosphiol. B Biol. 140 (2014) 344–358. https://doi.org/10.1016/j.jphotobiol.2014.07.021.
- [21] L.F. de Freitas, M.R. Hamblin Proposed Mechanisms of Photobiomodulation or Low-Level Light Therapy, IEEE J. Sel. Top. Quantum Electron. 22 (2016) 348–364. https://doi.org/10.1109/JSTQE.2716.2561201.
- [22] T. Karu, Mitochondrial Mechanisms of Photobiomodulation in Context of New Data About Multiple Roles of ATP, Photoccid. Laser Surg. 28 (2010) 159–160. https://doi.org/10.1080/pl o.2010.2789.
- [23] T.I. Karu, Cellular and Molecular Mechanisms of Photobiomodulation (Low-Power Laser Therapy), IEEE J. Sel. Tap. Quantum Electron. 20 (2014) 143–148. https://doi.org/10.1109/JSTQE.2013.2273411.
- [24] J.T. Eells, M.T.T. Wong-Riley, J. VerHoeve, M. Henry, E. V. Buchman, M.P. Kane, L.J. Gould, R. Das, M. Jett, B.D. Hodgson, Mitochondrial signal transduction in accelerated wound and retinal healing by near-infrared light therapy, Mitochondrion. 4 (2004) 559–567. https://doi.org/10.1016/j.mito.2004.07.033.
- [25] T.I. Karu, L. V. Pyatibrat, G.S. Kalendo, R.O. Esenaliev, Effects of monochromatic low-intensity light and laser irradiation on adhesion of HeLa cells in vitro, Lasers Surg. Med. 18 (1996) 171–177. https://doi.org/10.1002/(SICI)1096-9101(1996)18:2<171::AID-LSM7>3.0.CO;2-P.
- [26] T.I. Karu, Mitochondrial Signaling in Mammalian Cells Activated by Red and Near-IR Radiation, Photochem. Photobiol. 84 (2008) 1091–1099. https://doi.org/10.1111/j.1751-1097.2008.00394.x.

- [27] Y. Liu, G. Fiskum, D. Schubert, Generation of reactive oxygen species by the mitochondrial electron transport chain, J. Neurochem. 80 (2002) 780–787. https://doi.org/10.1046/j.0022-3042.2002.00744.x.
- [28] J.T. Hashmi, Y. Huang, B.Z. Osmani, S.K. Sharma, M.A. Naeser, M.R. Hamblin, Role of Low-Level Laser Therapy in Neurorehabilitation, PM&R. 2 (2010). https://doi.org/10.1016/j.pmrj.2010.10.013.
- [29] R. Giovannetti, The Use of Spectrophotometry UV-Vis for the Study of Porphyrins, in: Macro To Nano Spectrosc., InTech, 2012. https://doi.org/10.5772/38797.
- [30] J.L. Martin, M.H. Vos, Femtosecond Biology, Annu. Rev. Biophys. Biomol. Struct. 21 (1992) 199–222. https://doi.org/10.1146/annurev.bb.21.060192.001215.
- [31] M.H. Vos, Ultrafast dynamics of ligands within heme proteins, Biochim. Biophys. Acta Bioenerg. 1777 (2008) 15–31. https://doi.org/10.1016/j.bbabio.2007.10.004.
- [32] R. Berera, R. van Grondelle, J.T.M. Kennis, Ultrafast transient bsorption spectroscopy: principles and application to photosynthetic systems, Photosynth. Rev. 101 (2009) 105–118. https://doi.org/10.1007/s11120-009-9454-y.
- [33] A.P. Sommer, P. Schemmer, A.E. Pavláth, H.-D. Försterling Á.R. Mester, M.A. Trelles, Quantum biology in low level light therapy: death of a dog. a, Ann. Transl. Med. 8 (2020) 440–440. https://doi.org/10.21037/atm.2020.03.159.
- [34] A.A.P. Chauvet, A. Al Haddad, W.-C. Kao, F. van M. urik, C. Hunte, M. Chergui, Photo-induced dynamics of the heme centers in cytochron... bc 1, Phys. Chem. Chem. Phys. 17 (2015) 2143–2151. https://doi.org/10.1039/C4CP04805 \(\Lambda \).
- [35] M.H. Vos, B.J. Reeder, F. Daldal, U. Lital, "Iltrafast photochemistry of the bc 1 complex, Phys. Chem. Phys. 19 (2017) 6807–6813. https://doi.org/10.1039/C7CP00193B.
- [36] W. Wang, X. Ye, A.A. Demidov, F. Rosea, T. Sjodin, W. Cao, M. Sheeran, P.M. Champion, Femtosecond Multicolor Pump—Probe Spectroscopy of Ferrous Cytochrome c †, J. Phys. Chem. B. 104 (2000) 10789–10801. https://doi.org/10.1021/jp0008602.
- [37] M. Negrerie, S. Cianetti, M.H. Vo. Martin, S.G. Kruglik, Ultrafast Heme Dynamics in Ferrous versus Ferric Cytochrome a Studied by Time-Resolved Resonance Raman and Transient Absorption Spectroscopy, J. Phys. Chem. B. 110 (2006) 12766–12781. https://doi.org/10.1021/jp0559377.
- [38] D. Löwenich, K. Kleiner, Anns, V. Karunakaran, S.A. Kovalenko, Transient and stationary spectroscopy of cytochrone c ultrafast internal conversion controls photoreduction., Photochem. Photobiol. 84 (2008) 195–201. https://doi.org/10.1111/j.1751-1097.2007.00219.x.
- [39] M.H. Vos, G. Lipowski, J.-C. Lambry, J.-L. Martin, U. Liebl, Dynamics of Nitric Oxide in the Active Site of Reduced Cytochrome c Oxidase aa 3, Biochemistry. 40 (2001) 7806–7811. https://doi.org/10.1021/bi010060x.
- [40] V. V. Yakovlev, B. Kohler, K.R. Wilson, Broadly tunable 30-fs pulses produced by optical parametric amplification, Opt. Lett. 19 (1994) 2000. https://doi.org/10.1364/OL.19.002000.
- [41] K.R. Wilson, V. V. Yakovlev, Ultrafast rainbow: tunable ultrashort pulses from a solid-state kilohertz system, J. Opt. Soc. Am. B. 14 (1997) 444. https://doi.org/10.1364/JOSAB.14.000444.
- [42] T.F. Johnston, Beam propagation (M^2) measurement made as easy as it gets: the four-cuts method, Appl. Opt. 37 (1998) 4840. https://doi.org/10.1364/AO.37.004840.
- [43] P.J.M. Johnson, V.I. Prokhorenko, R.J.D. Miller, Stable UV to IR supercontinuum generation in calcium fluoride with conserved circular polarization states, Opt. Express. 17 (2009) 21488. https://doi.org/10.1364/OE.17.021488.
- [44] I.H.M. van Stokkum, D.S. Larsen, R. van Grondelle, Global and target analysis of time-

- resolved spectra, Biochim. Biophys. Acta Bioenerg. 1657 (2004) 82–104. https://doi.org/10.1016/j.bbabio.2004.04.011.
- [45] C. Ruckebusch, M. Sliwa, P. Pernot, A. de Juan, R. Tauler, Comprehensive data analysis of femtosecond transient absorption spectra: A review, J. Photochem. Photobiol. C Photochem. Rev. 13 (2012) 1–27. https://doi.org/10.1016/j.jphotochemrev.2011.10.002.
- [46] S.G. Kruglik, B.-K. Yoo, J.-C. Lambry, J.-L. Martin, M. Negrerie, Structural changes and picosecond to second dynamics of cytochrome c in interaction with nitric oxide in ferrous and ferric redox states, Phys. Chem. Chem. Phys. 19 (2017) 21317–21334. https://doi.org/10.1039/C7CP02634J.
- [47] Y. Wang, Y.-Y. Huang, Y. Wang, P. Lyu, M.R. Hamblin, Red (660 nm) or near-infrared (810 nm) photobiomodulation stimulates, while blue (415 nm), green (540 nm) light inhibits proliferation in human adipose-derived stem cells, Sci. Rep. 7 (20'7) 7781. https://doi.org/10.1038/s41598-017-07525-w.

Supplemental Information:

Contents:

S1. Determining Number of Replicate Scans

S2. TAS of reduced Cyt c using 418 nm pump

S1. Determining Number of Replicate Scans:

When using CW during TAS data collection, each scan will have undergone a different duration of CW illumination. Therefore, averaging each scan number with the same scan number from multiple other replicate data collections is necessary, instead of a reaging together all of the scans in one data collection. Since the signal to noise ratio is in portant for obtaining a good fit for the time constants with low uncertainty, we estimated 'nor many replicate data sets were necessary to average a sufficient number of scans between collections to reduce the noise sufficiently for fitting the data with the kinetic fit equation used in TAS analysis (Equation 1).

$$\Delta A_{\lambda}(t) = \sum_{i} A_{i} e^{-\frac{t-t_{0}}{\tau_{i}}} + A_{0} \#(1)$$

To estimate the number of data sets needed when using CW illuminations during TAS, a data collection with 20 scans was first taken or a sample of reduced cytochrome c without CW illumination. Then, a cross section was taken from each of the 20 sets of TAS data at the wavelength 430 nm which corresponded to a transient feature in the TAS data. The 20 cross sections were then used to compute a fer es of 20 averaged cross section beginning at 1 set and ending at 20 sets averaged together. Kinetic fits using equation 2 with two terms were then computed on each of the averaged cross sections. Then, the sum of squared residuals (SSR) was computed for each set and corresponding fit (Equation 2).

$$SS.' = ||r||_2^2 = \sum_i (A_{\lambda,fit}(t_i) - A_{\lambda,data}(t_i))^2 \#(2)$$

The SSRs were then normalized to the highest norm value and plotted as a function of the number of averaged sets. Thresholds were superimposed on the plot (Fig. S1c) to indicate where the norm has reduced to below 20% and 10% of the initial value from 1 scan.

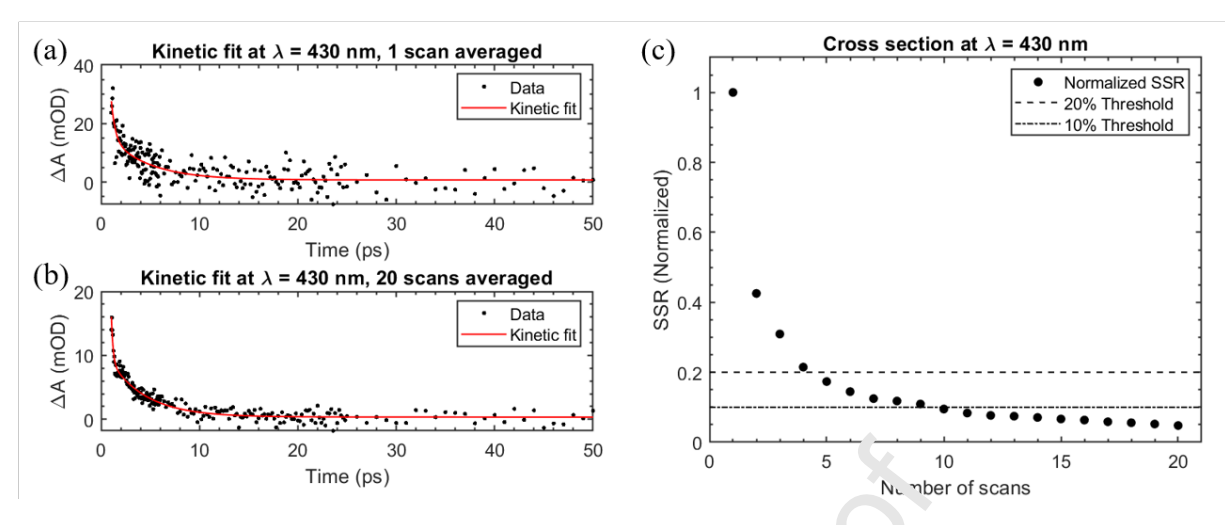


Fig. S1. Transient absorption data (black), along with kinetic fitting cu. ves (red) according to Eqn. 1, at 430 nm for cytochrome c with pump wavelength 418 nm are displayed vith (a) 1 scan averaged together and (b) 20 scans averaged together. (c) The SSRs of the fit and da a arriotted as a function of the number of scans averaged.

Figure S1 displays an analysis on reduced Cyt c using 2° scans without CW light to determine the number of replicate measurements that are needed for CW-TAS. Figure S1(a) and S1(b) are cross sections taken from reduced Cyt c's TAS dated the wavelength 430 nm, corresponding to a transient signal, after (a) 1 scan and (b) 2° a readed scans. For each set of averaged scans from 1-20, a kinetic fit was performed at 430 nm using Equation 2 with two terms. The SSR was computed using Equation 3 for each number of averaged scans and plotted in Figure S1(c). Approximately 5 scans were necessary to reduce the SSR, with respect to the data, to 20% while 10 scans were needed to reduce it below 10%.

Examining Figure S1(c), the SSK as a function of the number of averaged scans appeared to follow a decaying exponential tand. When performing this analysis at different wavelengths in the TAS data, the number of necessary scans can increase or decrease depending on experimental parameters. The intensity of the probe pulse, as well as the stability of its intensity, affect the signal to noise of the TAS data and hence the number of necessary replicate scans needed. This was necessary to reduce the error in fitting routines, such as kinetic analysis and singular value decomposition, which extract time constants from the TAS data and can have large standard deviations when the noise is significant.

S2. TAS of reduced Cyt c using 418 nm pump

Methods used to collect TAS data of Cyt c were the same as described in Section 2.2 of the main text with a few changes. The pump pulse generated from the 800 nm light source was split using an OPA and converted to 418 nm in this case in order to excite at the Soret band rather than at the Q band. Additionally, the supercontinuum was generated using the sapphire window rather than the CaF₂ window, in order to produce a supercontinuum that covers the visible (VIS) region as shown in Fig. S2.

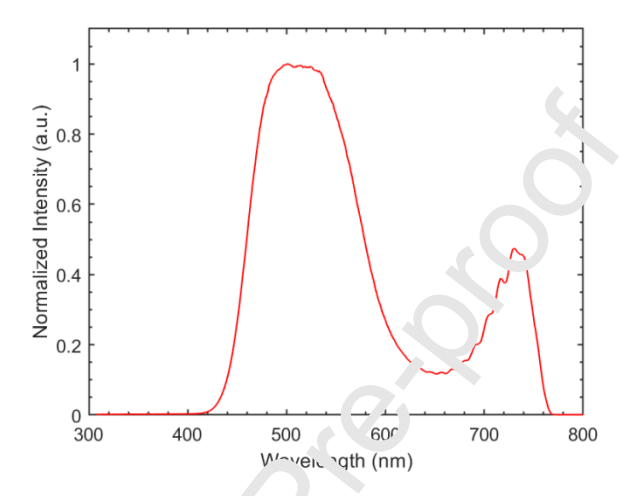


Fig. S2. Supercontinuum spertr. generated from the Sapphire window.

Figure S3 displays the resulting TAS at a of Cyt c using the 418-nm excitation wavelength and the VIS supercontinuum. Twenty-one stans were taken and averaged to produce the surface in Fig. S3a. Negative transients were absorped at 520 and 550 nm corresponding to the absorbance peaks in the Q band of Cyt c's grand state absorption spectra (Fig. 3), and therefore appear as ground-state bleaching in TAS. Additionally, the positive transients, with peaks at ~495 and 575 nm, observed on both sides of the Q band bleaching peaks corresponded to excited state absorptions.

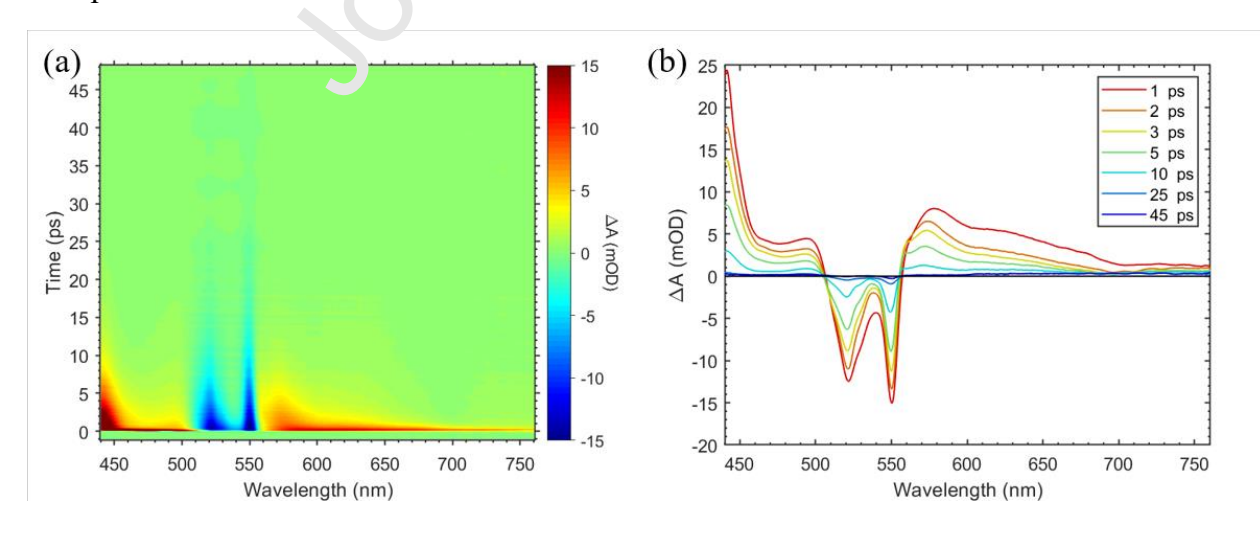


Fig. S3. Transient absorption spectra of cytochrome c with 418-nm excitation at 200 nJ/pulse displayed as a (a) surface and (b) spectral cross sections at different time delays.



Highlights

- Molecular mechanisms of photobiomodulation are studied using transient absorption spectroscopy for the first time
- A novel methodology transient absorption spectroscopy utilizing continuous wave excitation
- Extensive transient absorption studies of cytochrome c were performed
- Multiple photobiomodulation wavelengths used to study the effect of lirradiation on electronic processes in cytochrome c
- A possibility of electronic processes in cytochrome c being primarily involved in photobiomodulation has been eliminated